3-2022

Indocyanine-type Infrared-820 Encapsulated Polymeric Nanoparticle-Assisted Photothermal Therapy of Cancer

Ramesh Marasini

Santosh Aryal
University of Texas at Tyler, SantoshAryal@uttyler.edu

ACS OMEGA

http://pubs.acs.org/journal/acsodf

Article

Indocyanine-type Infrared-820 Encapsulated Polymeric Nanoparticle-Assisted Photothermal Therapy of Cancer

Ramesh Marasini and Santosh Aryal*

Cite This: *ACS Omega* 2022, 7, 12056−12065

Read Online

ACCESS | Metrics & More | Article Recommendations

ABSTRACT: Organic small-molecule photosensitizers are well-characterized and known for the light-responsive treatment modality including photodynamic therapy. Compared with ultraviolet−visible (UV−vis) light used in conventional photodynamic therapy with organic photosensitizers, near-infrared (NIR) light from 700 to 900 nm is less absorbed and scattered by biological tissue such as hemoglobin, lipids, and water, and thus, the use of NIR excitation can greatly increase the penetration depth and emission. Additionally, NIR light has lower energy than UV−vis that can be beneficial due to less activation of fluorophores present in tissues upon NIR irradiation. However, the low water stability, nonspecific distribution, and short circulation half-life of the organic photosensitizers limit its broad biological application. NIR responsive small-molecule fluorescent agents are the focus of extensive research for combined molecular imaging and hyperthermia. Recently a new class of NIR dye, IR-820 with excitation and emission wavelengths of 710 and 820 nm, has been developed and explored as an alternative platform to overcome some of the limitations of the most commonly used gold nanoparticles for photothermal therapy of cancer. Herein, we synthesized a core−shell biocompatible nanocarrier envelope made up of a phospholipid conjugated with poly(ethylene glycol) as a shell, while poly(lactic glycolic acid) (PLGA) was used as a core to encapsulate IR-820 dye. The IR-820-loaded nanoparticles were prepared by nanoprecipitation and characterized for their physicochemical properties and photothermal efficiency. These nanoparticles were monodispersed and highly stable in physiological pH with the hydrodynamic size of 103 ± 8 nm and polydispersity index of 0.163 ± 0.031. The IR-820-loaded nanocarrier showed excellent biocompatibility in the dark, whereas remarkable phototoxicity was observed with breast cancer cells (MCF-7) upon NIR laser excitation. Therefore, the IR-820-loaded phospholipid mimicking biodegradable lipid-polymer composite nanoparticles could have great potential for cancer theranostics.

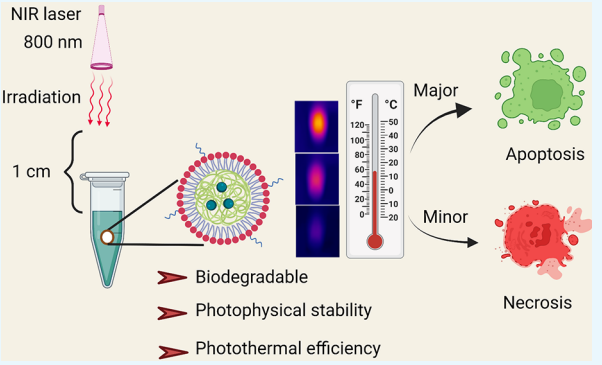

INTRODUCTION

With the progress of nanotechnology, there has been considerable attention in the treatment of cancer using thermal therapies such as magnetic hyperthermia, microwave-assisted hyperthermia, photosensitizer-induced photodynamic therapy, and plasmonic nanoparticle-mediated photothermal therapy (PTT) due to their high tumor ablation efficiency, good spatial resolution, and minimal side effects.[1−6] The most common feature in the aforementioned modalities is the use of heat energy to modulate cancer cells. Near-infrared (NIR) responsive fluorescent agents are the focus of extensive research for combined molecular imaging and hyperthermia. A key advantage of the PTT strategy is the fact that photothermal agents are capable of annihilating cancer cells with remote light irradiation while causing minimal damage to normal tissues.[6] On the one hand, in contrast to inorganic nanoparticles such as super-paramagnetic iron oxide nanoparticles and gold nanoparticles, NIR-absorbing small-molecule organic dyes overcome the issue of metal-induced toxicity such as redox-active and unknown metabolic pathways when incorporated in a suitable envelope and thus are generally considered to be more biocompatible.[7−12] On the other hand, optical imaging is inexpensive with good resolution, easy to handle, and can be made portable offering broad application when compared to other modalities such as magnetic resonance imaging, computed tomography, or positron-emitting tomography,[13−15] thanks to the advancement in fiber optics technology that makes optical imaging ideal for incorporation into an endoscope used in minimally invasive procedures. However, conventional optical imaging that uses the light of lower wavelengths in the ultraviolet−visible (UV−vis) region suffers due to high light scattering and absorption by tissues.[16] Instead, NIR light of

Received: January 15, 2022
Accepted: March 7, 2022
Published: March 28, 2022

wavelengths from 700 to 900 nm has a deep tissue penetration limit owing to minimal scattering and tissue absorption.[17] Small organic molecule fluorescent probes that absorb energy in the NIR region will release vibrational energy in the form of heat following exposure to light illumination and can kill cancer cells similar to that of plasmonic PTT mediated by noble-metal nanoparticles.[13]

Indocyanine green is a tricarbocyanine-type dye with NIR-absorbing properties approved for visualization of retinal and choroidal vasculature, blood volume determination, and photodynamic therapy.[11,12,18,19] However, the low water stability and short circulation half-life limit its broad application for hyperthermia and in vivo imaging.[20] To address these issues, the use of IR-820 dye as a potential alternative has been described in the literature.[7,21−25] IR-820 dye has similar structural and optical characteristics to those of indocyanine green with a relatively longer absorption range through maximal excitation and emission wavelengths of 710 and 820 nm, respectively. Prajapati and colleagues reported the use of IR-820 as a blood pool contrast agent to image tissue injuries and tumors in mice with improved circulation half-life compared to the indocyanine green.[25] In an in vivo study by Pandey and colleagues, they conjugated IR-820 with a photodynamic therapy drug and studied its potential for dual imaging and thermotherapy.[26] Although these reports indicate that IR-820 has the potential for in vivo applications and provides an attractive alternative to metallic nanoparticles, there is still more for the field to provide a detailed in vitro characterization regarding its photothermal efficiency and cellular behavior in nanoformulations.

When an NIR dye, as an organic photothermal agent, is encapsulated into a suitable delivery vehicle, it can be selectively activated by the external stimulus such as light after the dye has reached its intended target, for example, tumor offering an image-guided treatment platform. The incorporation of the photothermal agent into self-assembled polymeric nanocarriers confers several benefits to PTT including biodegradability, scalability, and reproducibility.[26−29] Herein, we designed a lipid polymer-based core−shell nanocarrier by encapsulating the indocyanine class of IR-820 dye into the polymeric form for the photothermal treatment of breast cancer. These lipid−polymer hybrid nanocarriers delivered IR-820 to MCF-7 breast cancer cells as a potent mediator of PTT exhibiting significant cytotoxic effects upon excitation with a clinically approved external laser light stimulus. The results also showed that these NPs induced cell death primarily through apoptosis, a preferred cell-death pathway over necrosis that may lead to the recurrence and metastasis of tumors.[30] With the great success of photothermal cancer treatment in vitro, this approach exhibits promising potential for in vivo applications. Furthermore, the photothermal treatment modality could be improved by combining NIR-responsive agents with anticancer drugs or photosensitizers for combination therapy like photothermal−chemotherapy or photothermal−photodynamic therapy to maximize their therapeutic efficacy with a synergistic cancer treatment.

MATERIALS AND METHODS

Chemicals and Reagents. Carboxylic end group terminated PLGA (lactide/glycolide = 50:50 dL g^{-1}) was purchased from the DURECT Corporation and used after purification by repeated precipitation in diethyl ether. 1,2-Distearoylphosphatidylethanolamine poly(ethylene glycol succinyl) (DSPE-PEG-COOH), 1,2-distearoyl-*sn*-glycero-3-phosphoglycerol, sodium salt (DSPG), and phospholipid conjugated l-α-phosphatidylethanolamine-*N*-(lissamine rhodamine-B sulfonyl) (ammonium salt) (RhB) was purchased from Avanti Polar Lipid Inc. (Alabaster) and used as received. 4′,6-Diamidino-2-phenylindole dihydrochloride (DAPI), (3-(4,5-dimethylthiazol-2-yl)-2,5-diphenyl tetrazolium bromide) (MTT), acetonitrile, and dimethyl sulfoxide (DMSO) were purchased from Sigma-Aldrich. IR-820 (CAS No. 172616-80-7) dye was purchased from BOC Sciences, and Annexin V/propidium iodide (PI) stain was purchased from BD Bioscience. All other analytical grade reagents and solvents were used without further purification.

Human breast cancer (MCF-7) and Dulbecco's Modified Eagle's Medium (DMEM) were purchased from American Type Cell Culture (ATCC). Fetal bovine serum (FBS) USDA Premium Select, heat-inactivated, was purchased from MIDSCI. Cells were maintained in DMEM supplemented with 10% (v/v), FBS and 1% streptomycin at 37 °C in a 5% CO_2 environment. When cells reached 80−90% confluency in T75 cell culture flasks, they were passaged or plated by detaching the cells from the flask using Trypsin−ethylenediaminetetraacetic acid (EDTA) (Thermo Fisher) and then counting the cells with a hemocytometer. The cell lines were used from passage 10 for bionano interaction studies.

Preparation of IR-820 Encapsulated Nanoparticles. PLGA with a carboxylic acid-terminated end group of molecular weight 50 kDa was used to synthesize IR-820 encapsulated PLGA nanoparticles following the well-established nanoprecipitation protocol.[31−38] In a typical experiment, the calculated amount of IR-820 in DMSO was physically adsorbed with 1 mg of PLGA in acetonitrile and made the final volume of the mixture to 1 mL to prepare IR-820-encapsulated PLGA nanoparticles. Then the phospholipids that consist of lipid mixture formulations having 260 μg of DSPE-PEG and 200 μg of DSPG were used in 4% ethanol, respectively. This lipid mixture was stirred at 60 °C for 30 min, and then an IR-820 encapsulated PLGA nanoparticle solution was added dropwise to the lipid suspension with stirring followed by the addition of 1 mL of deionized water (acetonitrile/water = 1:3). The content was further stirred at room temperature for 1 h to facilitate the formation of nanoparticles. The IR-820 encapsulated PLGA nanoparticles thus formed were purified using a 10 kDa Amicon wash at 3500 rpm for 10 min. The washing was done three times in 1X phosphate-buffered saline (PBS), made to a final concentration of 1 mg/mL in 1X PBS, and stored at 4 °C until further use. Similarly, control nanoparticles were prepared in the same phospholipid ratio and PLGA content without IR-820.

Characterization of Nanoparticles. The morphology of the purified NPs was characterized using a transmission electron microscope (TEM) (FEI Technai G2 Spirit BioTWIN). TEM samples were prepared by incubating 20 μL of IR-820 PLGA NPs (1 mg/mL) with 20 μL of 0.1% uranyl acetate for 5 min at room temperature. The sample was then placed on a Formvar-coated copper grid (400 mesh) and let stand for an additional 20 min. The excess amount of sample was removed before image acquisition. TEM images were acquired at 120 kV and analyzed by the GATAN digital imaging system (GATAN, Inc.). Similarly, NPs were characterized for hydrodynamic size and zeta potential measurements using a Malvarian Zeta sizer Nano. In this instrument, the Brownian motion and the Smoluchowski equation were used to calculate the average hydrodynamic size and zeta potential value, respectively. The colloidal stability of

https://doi.org/10.1021/acsomega.2c00306
ACS Omega 2022, 7, 12056−12065

NPs was investigated in both ionic and serum conditions to mimic the biological environment. In brief, 1 mg of NPs dispersed in the medium was subjected to a hydrodynamic size analysis over the period to obtain size, polydispersity index (PDI), and zeta potential values. The reported intensity-based hydrodynamic diameter is the *z*-average of three measurements, while the total count-based zeta potential is also the average of three measurements. The formulation with low PDI, high stability, and uniform narrow size distribution was selected for the in vitro application. Likewise, the stability of IR-820 dye in NPs was studied by mixing 500 μL of IR-820 encapsulated NP and 500 μL of 1X PBS (n = 3) over the period to ensure the dispersity and colloidal stability of NPs in physiological media. The size and PDI of the particles after being dispersed in PBS was measured each day for a week using dynamic light scattering (DLS).

The optical properties of IR-820 PLGA NPs were characterized by ultraviolet−visible spectrophotometry (BIOMATE-3S, Thermo Scientific) with 1.0 mm path length quartz cuvettes based on reading the absorbance of the NPs at 710 nm and comparing to a standard curve of known dye concentration dissolved in DMSO with dilution as required. The samples were scanned from 400 to 1100 nm with a baseline correction. The amount of IR-820 released from the NPs while in storage conditions was also examined by UV−vis spectroscopy. At several time points between 0 and 7 d post preparation, samples were centrifuged using a 10 kDa Amicon filter to separate the NPs from released IR-820, and the collected released IR-820 was compared to a standard curve of known dye concentration using the same scanning conditions as described above. The dye release study was performed three times, and the average and standard deviation of all three trials are reported.

For the IR-820 dye loading and release study, IR-820 was loaded on PLGA NPs by the direct mixing of a known concentration of dye into the PLGA polymer followed by the nanoprecipitation technique.[39−42] To optimize the maximum IR-820 loading, different calculated amounts such as 150, 300, and 400 μg of IR-820 were initially fed with 1 mg of PLGA dissolved in 400 μL of acetonitrile solution. The amount of encapsulated IR-820 was quantified, after purification, spectrophotometrically using a UV−vis spectrophotometer by measuring the absorbance of the NPs at 710 nm. The drug loading efficiency was calculated using the following equation.

$$\%\text{loading efficiency} = (\text{amount of encapsulated IR-820/amount of initial IR-820input}) \times 100$$

The cumulative free IR-820 dye release from IR-820 PLGA NPs and free IR-820 (Mw = 849.47) was studied using 3.5 kDa molecular cutoff dialysis bags at physiological pH (pH 7.4, PBS). For this purpose, 300 μg of IR-820 input formulation was selected for further studies due to the stable physiochemical properties. Free IR-820 release from selected formulations was tracked throughout 72 h by dialysis. One milliliter of IR-820 PLGA containing 1 mg/mL of NPs or an equivalent concentration of free IR-820 dye was dialyzed in 200 mL of PBS release media kept at 37 °C, while constant stirring (80 rpm) was maintained to retain the sink condition during the experiment. One milliliter of release media was taken at a regular interval and replaced with equivalent fresh media. The amount of free IR-820 in the release media was quantified spectrophotometrically, and the cumulative release percentage was calculated using the following equation.

$$\%\text{cumulative IR-820 release} = (\text{IR-820 in release media/IR-820 in 100\%release}) \times 100$$

The photothermal efficiency of free IR-820 and IR-820 PLGA NPs was measured in an aqueous suspension upon 808 nm laser (China Deheng Group, Inc.) irradiation with a thermal camera imaging system (Forward Looking InfraRed FLIR A5 systems). Samples were suspended in PBS at an IR-820 concentration of 20−120 μM with a total volume of 1 mL in the Eppendorf tube. The free dye and IR-820 PLGA NPs were then irradiated with a continuous-wave constant diode laser power of 808 nm laser for 2 min at varying power densities from 5.3 to 21.2 W/cm^2 while maintaining an ∼1 cm distance between the laser and sample. The concentration dependence of the photothermal efficiency for IR-820 PLGA NPs was examined by irradiating nanoparticles at concentrations of 20, 60, or 120 μM of IR-820 content with the 808 nm laser set to different power densities for 2 min. The temperature in each sample was recorded once every 30 s during irradiation, and the experiments were repeated three times. To further evaluate the influence of NIR laser exposure on the optical and physical properties of the NPs, we recorded the absorbance spectra, hydrodynamic diameter, and polydispersity index of IR-820 PLGA NPs by UV−vis spectroscopy and DLS both before and after irradiation.

Cellular Biocompatibility and NIR-Mediated Phototoxicity Study. The in vitro biocompatibility of free IR-820 dye and IR-820 PLGA NPs was conducted in MCF-7 cells using a colorimetric assay for assessing cell metabolic activity by an MTT assay. A time-dependent MTT assay in dark was conducted as discussed in the literature.[43−46] In brief, cells at a density of 1 × 10^4 cells per well in a 96-well plate were incubated overnight. The seeded cells were washed twice with 1X PBS to remove the debris before NPs treatment. Then the medium was replaced with various concentrations of NPs (0.01, 0.1, 0.5, 5, 10, 25, 50,100, 200 μg/mL) suspended in DMEM. The control cell was maintained without treatment. After 24 h of incubation, cells were washed with 1X PBS to remove surface-absorbed and excess NPs. After the washing, 100 μL of MTT (5 mg/mL in PBS, filtered through a 0.22 μm syringe) reagent was added to each well following the manufacturer's recommendation. Then the supernatant was aspirated followed by the addition of 100 μL of DMSO for solubilizing formazan crystal. The plate was gently shaken in an orbital shaker for 5 min in the dark, and absorbance was recorded at 560 nm using a microplate reader (BioTek, Synergy H1 hybrid reader). To analyze the data, the background (DMSO only) was subtracted from the absorbance reading in each well. Triplicate well signals were averaged and then normalized to untreated cells. These experiments were performed in triplicate and analyzed by Student's *t*-tests at each concentration.

The in vitro phototoxicity of IR-820 or IR-820 PLGA NPs was conducted in cells seeded as described above and treated with IR-820 PLGA NPs at the IR-820 concentration of 60 μM or with fresh media for 24 h of incubation at 37 °C. The cells were then washed with PBS and incubated in fresh media for 1 h to bring the temperature to 37 °C. The appropriate wells were then irradiated with continuous-wave 808 nm light at 14.1 W/cm^2 for 30 s/well such that the treatment groups included no treatment, laser light only, IR-820 PLGA NPs only, or IR-820 PLGA NPs with laser light with an ∼1 cm distance between the laser and sample. The irradiation was performed at room temperature, and the sample was returned to the 37 °C incubator immediately

https://doi.org/10.1021/acsomega.2c00306
ACS Omega 2022, 7, 12056−12065

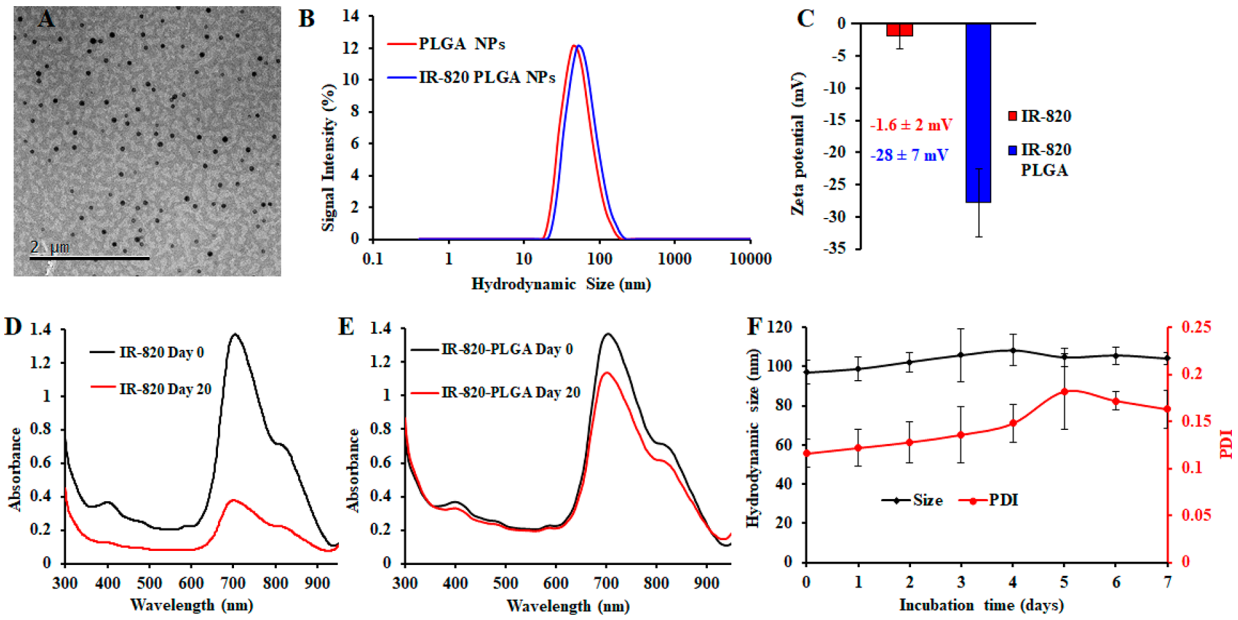

Figure 1. Morphology, size, and photostability of IR-820-PLGA NPs. (A) TEM image of IR-820-PLGA NPs. (B) Hydrodynamic size with different initial input of IR-820 concentration (150−400 μg) per milligram of PLGA NPs. (C) Zeta potential of IR-820 and IR-820 PLGA NPs. (D, E) Optical properties (absorption profiles) of free IR-820 dye and IR-820 PLGA NPs in water before and after storage at 4 °C, as determined by UV−vis spectrophotometry. The concentration of IR-820 is 60 μM (corresponding to 300 μg input) for both free and encapsulated dye. (F) Stability of particles over storage. Data represent n = 3.

following irradiation. After 24 h, the MTT assay was performed as described above. Data obtained were compared side-by-side with the control experiment to map the relative toxicity. Data shown are from three experiments that were each run with triplicate wells, and the data were analyzed by a one-way analysis of variance (ANOVA) with post hoc Tukey.

Intracellular Uptake Study. To evaluate the cellular internalization competence of IR-820 PLGA NPs, experiments were conducted with MCF-7 cells using confocal microscopy and flow cytometry studies.[47] For the confocal study, cells were seeded on poly-D-lysine-coated eight-chamber slides at a density of 50 000 cells per well and incubated for 24 h. Then the cells were treated with 50 μg/mL rhodamine-lipid labeled IR-820 PLGA NPs suspension prepared in complete DMEM and incubated for 3 h. After the incubation, the treated cells were washed twice with 1X PBS (pH = 7.4) and fixed with 4% paraformaldehyde for 30 min at room temperature. The nucleus of the cells was stained with DAPI for an additional 10 min and imaged under a confocal laser scanning microscope (Carl Zeiss, CLSM-700). Cells without any treatment served as control cells. The quantitative percentage of fluorescence intensity was determined using the Image-J software. The quantification of the intensity of internalized RhB-lipid labeled NPs was calculated in terms of corrected total cell fluorescence (CTCF) by use of the following equation.

$$\text{CTCF} = \text{integrated density} - (\text{area of selected cell} \times \text{mean fluorescence of background readings})$$

To investigate the quantitative cellular uptake of IR-820 PLGA NPs, a fluorescence-activated cell sorting (FACS) study was conducted after we labeled NPs with rhodamine B-lipid dye using lipid insertion followed by the nanoprecipitation technique described above.[31,32,46] In brief, MCF-7 cells with passage 10 were plated at the density of 1×10^5 cells per well on poly-D-lysine-coated 24-well plates and incubated overnight. Cells were then treated with 0, 20, or 60 μM IR-820 content in IR-820 PLGA NPs prepared as described above and incubated for 3 h to evaluate dose dependency. After 3 h, the cells were rinsed with 1X PBS, lifted off the plate with Trypsin−EDTA, and resuspended in 500 μL of 1X PBS to yield a single cell suspension of 1×10^6 cells that were analyzed by BD LSR Fortessa X-20 Special Order Research Product Flow Cytometer. Control cells were maintained without any treatments. 10 000 gated events were collected for all measurements. Density plots showing forward and side scatter data were used to create a primary gate for cells, excluding debris, prior to analyzing IR-820 PLGA NPs content.

Investigation of the Mechanism of Cell Death Induced by PTT. To analyze the mechanism of cell death induced via PTT mediated by IR-820 PLGA NPs, cells were seeded at 3×10^5 cells per well in a 24-well plate and incubated overnight. Cells were then treated with 20 μM of IR-820 content in IR-820 PLGA NPs for 3 h, at which time the cells were rinsed with 1X PBS and the wells were replenished with fresh media. The appropriate wells were then irradiated with continuous-wave 808 nm light at 14.1 W/cm^2 for 30 s per well for the following groups of samples: no treatment, cells with laser light only, IR-820 PLGA NPs only, or IR-820 PLGA NPs with laser light. After the laser light treatment, the samples were returned to the incubator. After 24 h, an Annexin V/PI staining was conducted as per the manufacturer's recommendations. Briefly, cells were lifted from the plate with Trypsin−EDTA, washed with 1X binding buffer, and resuspended in 100 μL of binding buffer containing 1:500 Annexin V and 1:1000 PI stains for 15 min in the dark condition. The samples were then diluted with 300 μL of 1X binding buffer and analyzed on the BD LSR Fortessa X-20 Special Order Research Product Flow Cytometer with FITC (excitation, 488 nm; emission, 530/30 nm) and PerCP (excitation, 488 nm; emission, 675/30 nm) channels. Density plots showing forward and side scatter data were used to create a primary gate for cells, excluding debris, before establishing gates

https://doi.org/10.1021/acsomega.2c00306
ACS Omega 2022, 7, 12056−12065

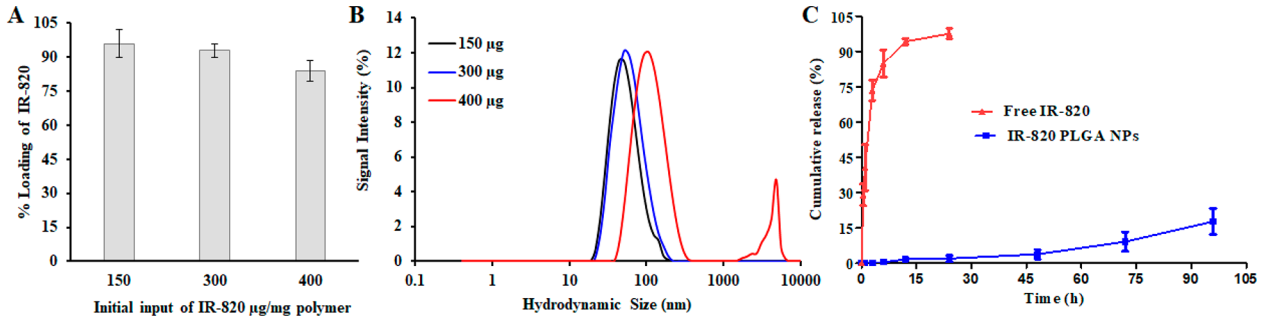

Figure 2. IR-820 loading and release study. (A) IR-820 loading into PLGA NPs. (B) Hydrodynamic size with different initial input of IR-820 concentration (150−400 μg) per milligram of PLGA NPs. (C) Cumulative dye-release kinetics from free IR-820 and IR-820 PLGA NPs at physiological condition (PBS at pH 7.4). The concentration of IR-820 is 60 μM (corresponding to 300 μg input) for both free IR-820 and IR-820 PLGA NPs. Data represent n = 3.

for Annexin V-positive and PI-positive cells. 10 000 gated events were collected for all measurements. Positively stained gates were based on unstained cells, and single-stained controls including Annexin V only, PI only, or free IR-820 dye were used for compensation. The data presented are the average of three experiments and were analyzed by one-way ANOVA.

Data and Statistical Analysis. The obtained data were plotted and compared to the significance of the results using GraphPad software. Different statistical models and tests were performed including a t-test, F-test, and dose−response inhibition model fit using GraphPad software according to the requirement. All data represent the mean ± standard deviation. Biocompatibility and cytotoxicity data include six replicates (n = 6). All other major data include at least three replicates (n = 3).

RESULTS AND DISCUSSIONS

Physiochemical Characterization. The nanoparticles were fabricated using the nanoprecipitation technique. The morphology of IR-820 PLGA NPs was characterized by TEM and DLS, which showed that the nanoparticles were spherical, uniformly distributed, and had the hydrodynamic diameter of 103 ± 8 nm (Figure 1A,B). The encapsulation of IR-820 dye has no significant impact in the diameter of nanoparticles as compared to the control particles without dye, which has a size of 96 ± 3 nm. These nanoparticles were negatively charged with a zeta potential value of −28 ± 7 mV (Figure 1 C), as compared to the slightly negative charge (−1.6 ± 2 mV) of free IR-820 in aqueous condition. No significant change in the surface zeta potential further assured us that the IR-820 dye is loaded into the core of the NP. The negative charge in IR-820 PLGA NPs is due to the presence of the carboxylic acid-terminated phospholipid PEG moiety. The optical property of the particles including free IR-820 and IR-820 PLGA NPs by using UV−vis spectroscopy revealed a characteristic extinction spectrum peak at 710 nm of free dye that is shifted further to the longer wavelength by 15 nm, red-shift, after loading into the nanoparticles (Figure 1D,E). To evaluate the stability and retention of optical properties of IR-820 dye free in solution or loaded into the NPs, we analyzed the extinction spectrum of freshly prepared samples and samples that had been stored at 4 °C for three weeks. After storage in MilliQ water, we observed that free IR-820 dye loses its absorption capabilities, whereas IR-820 PLGA NPs fairly maintain their optical properties (Figure 1D,E). To further examine the stability of IR-820-loaded PLGA NPs, we evaluated the colloidal stability by monitoring the hydrodynamic size and PDI up to 7 d as shown in Figure 1F. During 7 d of incubation time, the PDI of NPs varied from 0.116 to 0.163, and the size varied from 97 to 108 nm. Taken together with optical properties, these characterization data show minimum variation during the storage condition signifying better stability and the retention of dye in the NPs compared to the free dye solution.

Next, we studied the dye loading and release kinetics to explore the potential application of IR-820 in the drug delivery platform for PTT. IR-820 dye was used as a photoresponsive agent. The IR-820 dye was loaded into PLGA NPs using the lipid insertion mediated nanoprecipitation technique. As shown in Figure 2A, the percentage loading efficiency of dye with respect to the various initial input concentrations of dye was calculated. Our synthetic protocol yielded a high loading efficiency of 84%−96% with input IR-820 concentration ranging from 400 μg to 150 μg/mg polymer, respectively. Unfortunately, in the case of high loading content with 400 μg, IR-820 is aggregated, as observed from the increased size and bimodal distribution (Figure 2B). However, in the case of 300 μg IR-820 initial input, the size and PDI of NPs after loading (103 nm, 0.135 PDI) was similar to that before loading (96 nm, 0.112 PDI), as shown in Figure 1B. Also, the loading efficiency was 93%, and the percentage of dye content (%wt) to the carrier was 1.37%. So, among the different formulations studied, it was found that 300 μg/mg polymer showed the best stability in media while maintaining its loading content. Therefore, we chose the 300 μg/mg polymer input formulation as a standard for further experiments. No significant changes in the size and PDI of this formulation were observed when incubated at 37 °C for 7 d in PBS (pH = 7.4), confirming the excellent physicochemical properties (Figure 1F). To determine the release efficiency of the dye from the NPs, 2 mL samples of 1 mg/mL were placed in a dialysis bag and processed under identical conditions. We observed burst and sustained dye-release kinetics for free IR-820 and IR-820 PLGA NPs over a 72 h period at 37 °C (pH = 7.4), respectively. On the one hand, the results, as shown in Figure 2C, indicate that ∼36% IR-820 was released within a period of 1 h, while, over 12 h, we observed ∼90% in dye-release kinetics. On the other hand, we found a higher order of dye stability in the IR-820 PLGA NPs. Less than 20% of IR-820 was released throughout the release study period of 72 h. These data are consistent with the literature with the release of similar lipophilic dyes such as DiR dye or indocyanine green from the nanoparticles.[22,25,39,40,48] The stability of the dye is highly essential in device NPs for a theragnostic application.

IR-820-Mediated Photothermal Efficiency. The concentration dependence and laser power dependence photothermal efficiencies of free IR-820 and IR-820 PLGA NPs were

https://doi.org/10.1021/acsomega.2c00306
ACS Omega 2022, 7, 12056−12065

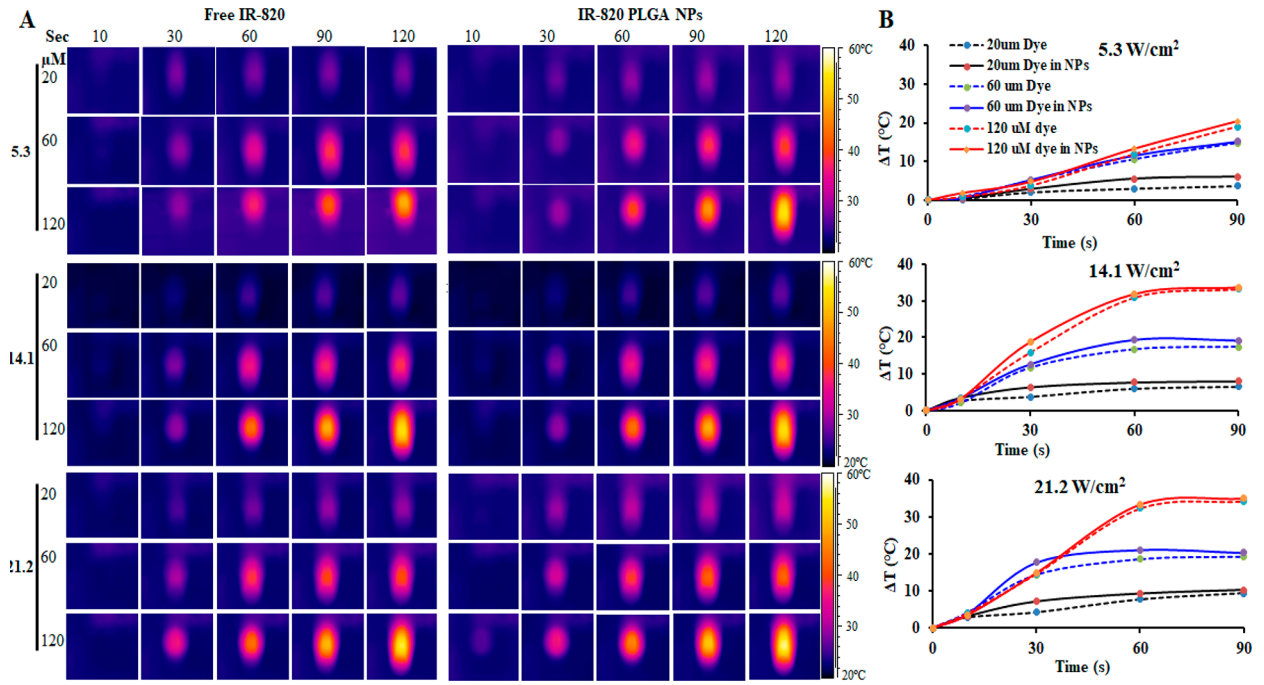

Figure 3. Comparative photothermal efficiency of free IR-820 dye and IR-820 PLGA NPs. (A) The concentration and power-dependent NIR laser (λ = 808 nm) heating thermograph profile of IR-820 PLGA NPs and free IR-820 dye suspension upon laser irradiation. Three different laser power densities 5.3, 14.1, and 21.2 W/cm^2 and 20, 60, and 120 μM IR-820 dye corresponding to 150, 300, and 400 μg input/mg polymer were irradiated for 2 min with the laser-to-sample distance of ∼1 cm. The evolution of temperature throughout the suspension was recorded using an FLIR thermal camera system. (B) The corresponding temperature plots showing the average change in temperature as a function of time from (A). Data represent n = 3.

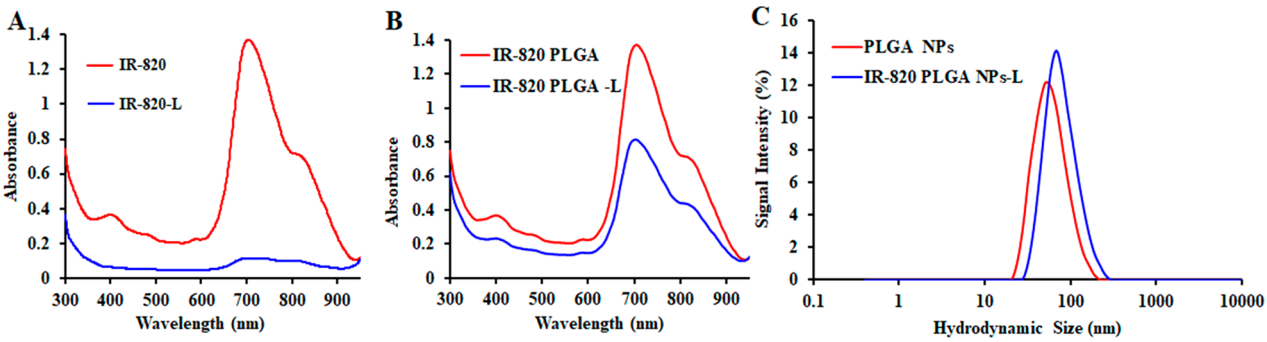

Figure 4. Optical response and alteration in the size of IR-820 PLGA NPs after laser exposure. (A, B) UV−Vis absorption profile showing the changes in optical density of free IR-820 dye and IR-820 PLGA NPs before and after laser irradiation. (C) Changes in the hydrodynamic size of PLGA NPs and IR-820 PLGA NPs after laser exposure measured by DLS. These data were recorded for the laser power density of 14.1 W/cm^2 and 60 μM IR-820 dye content either in free dye or in NPs that were irradiated for 2 min.

investigated under 808 nm NIR laser irradiation using three different concentrations of IR-820 from 20 to 120 μM and power densities of 5.3, 14.1, and 21.2 W/cm^2. All samples suspended in an aqueous solution were irradiated where the change in temperature versus time was noted using a thermal imaging system at an interval of 30 s. As shown in Figure 3, a time-dependent increase in temperature was observed in all samples. As expected, we observed low heat evolution at a lower concentration of dye or laser power used for both samples. However, we did not observe any bigger difference in the temperature rise between free IR-820 dye or IR-820 PLGA NPs at an identical dye content. As a general trend, we found that IR-820 PLGA NPs produced more temperature compared to the free IR-820 under identical conditions of dye concentration and laser power used (Figure 3A,B). At 5.3 W/cm^2, free IR-820 increased the temperature (ΔT) from 3.7 to 19 °C, while IR-820 PLGA NPs increased from 6 to 20.4 °C under similar dye content ranging from 20 to 120 μM. The temperature was increased from 6.5 to 33.3 °C and from 8 to 33.6 °C while from 9.4 to 34.2 °C and from 10.2 to 35 °C for free IR-820 and IR-820 PLGA NPs at 14.1 and 21.2 W/cm^2, respectively. Interestingly, we did not find a significant difference in heat evolution at 14.1 versus 22.2 W/cm^2 irrespective of the sample. To investigate the effect of laser exposure to the optical and physicochemical properties of IR-820 PLGANPs or free IR-820, we recorded the UV−vis spectra and size of the particles. We observed a significant reduction in the absorption peak of free IR-820 but a lesser effect of laser in the case of IR-820 PLGA NPs after a laser exposure of 2 min (Figure 4A,B). As shown in Figure 4C, we did not have much effect on laser irradiation in terms of size and PDI of the IR-820 PLGA NPs. However, during the NIR exposure, a change in the color of the free IR-820 suspension was observed, which was confirmed by recording the change in optical density and absorption peak, as can be seen in Figure 4A. This is

https://doi.org/10.1021/acsomega.2c00306
ACS Omega 2022, 7, 12056−12065

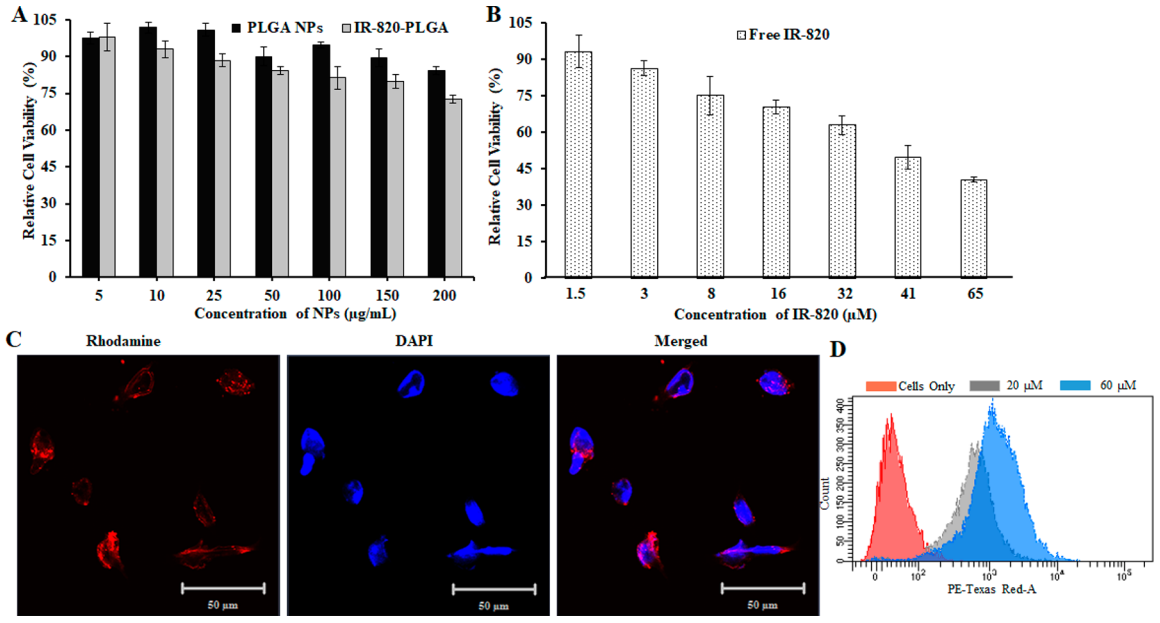

Figure 5. Cellular interaction study in MCF-7 cells. (A) Concentration-dependent relative cell viability of MCF-7cells exposed to PLGA NPs or IR-820 PLGA NPs without light exposure. (B) Concentration-dependent cell relative viability of MCF-7 cells exposed to free IR-820 dye. The concentration of IR-820 was used similar to the IR-820 content encapsulated in PLGA NPs as shown in (A). (C) Confocal microscopic micrographs capture Rh−B-lipid labeled IR-820 PLGA NPs cellular internalization at 3 h of incubation, and (D) corresponding FACS analysis (Data represent $n = 6$ for biocompatibility and $n = 3$ for FACS study).

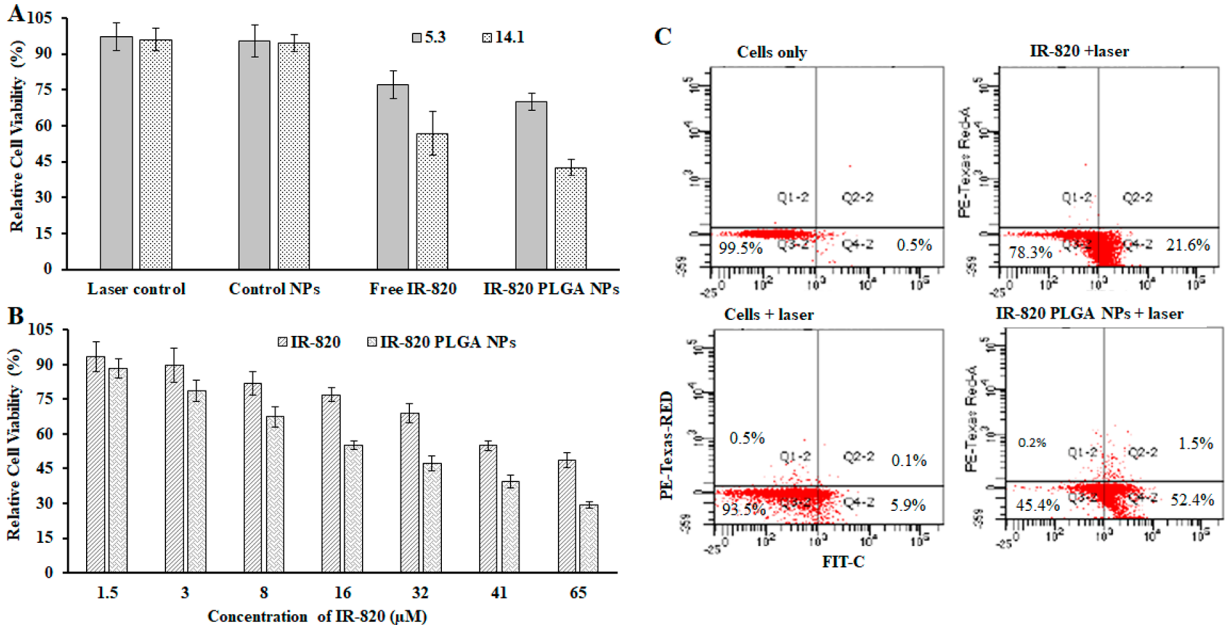

Figure 6. NIR-mediated phototoxicity study and its mechanism of cell death in MCF-7 cells. (A) A comparative power-dependent PTT using either cells, PLGA NPs, free IR-820, or IR-820 PLGA NPs (60 μM) with laser exposure for 30 s. These data were recorded for the laser power density of 5.3 vs 14.1 W/cm^2, respectively, to map the best power density for further investigation. (B) A comparative dose-dependent relative phototoxicity of MCF-7 cells after photothermal therapy generated by free IR-820 vs IR-820 PLGA NPs having identical dye content after 808 nm laser exposure for 30 s at 14.1 W/cm^2. (C) A representative scatter plot demonstrating the fraction of cells in early apoptosis (bottom right quadrant), late apoptosis (top right quadrant), or necrosis (top left quadrant) following treatment with media only, cells + laser, IR-820-PLGA NPs only, or IR-820-PLGA NPs + laser.

presumably because the aqueous stability of IR-820 is greatly affected by the local temperature, and a high local temperature makes free dye unstable in the suspension. In contrast to free IR-820, the retention of optical density and higher order of colloidal stability was observed in the case of IR-820 PLGA NPs. These results demonstrate that IR-820 PLGA NPs could act as an excellent photothermal source for therapeutic study.

Biocompatibility and Cellular Internalization Study. The biocompatibility of free IR-820 and IR-820 PLGA NPs was assessed in human breast cancer cell MCF-7 as presented in Figure 5A,B for 48 h of treatment. The IR-820 dye concentration as a handle was used to assess the biocompatibility. IR-820 PLGA NPs showed at least 80% cell viability (Figure 5A) at a high concentration (200 μg/mL), while the viability of free IR-

https://doi.org/10.1021/acsomega.2c00306
ACS Omega 2022, 7, 12056−12065

820 was found to be 42% at an equivalent concentration (65 μM of IR-820), (Figure 5B). The dye concentration was used according to the dye content in nanoparticles used in Figure 5A. These data signify the biocompatibility of IR-820 PLGA NPs even at high concentrations. We further extended our approach to see if IR-820-loaded NPs were taken up by cells. We labeled IR-820 PLGA NPs with Rh−B-lipid, treated with cells for 3 h, and found that these nanoparticles were taken up by cells (Figure 5C). To further evaluate the dose dependency and quantitative cellular uptake of the same Rh−B-lipid-labeled nanoparticles upon treatment and incubation for 3 h with an IR-820 concentration of 20 or 60 μM, an FACS study was performed. As shown in Figure 5D, nanoparticles were taken up by the cells, and as expected, we observed that a significantly larger amount of IR-820 PLGA NPs was taken up by cells when treated with 60 μM IR-820 content. It is worth mentioning that this concentration of nanoparticles is well-tolerated with more than 70% of cells being viable even at the large concentration input of 200 μg/mL (Figure 5A). Taken together, these observations reflect excellent biocompatibility and uptake of IR-820 PLGA NPs signifying that it can be used as a safe photothermal delivery agent.

NIR-Mediated Phototoxicity Study. We next investigated the use of IR-820 PLGA NP-mediated PTT as a treatment strategy for breast cancer and probed the mechanism of cell death induced by this treatment modality. MCF-7 cells were treated with 60 μM dye in IR-820 PLGA NPs, the maximum tolerated dose determined previously (Figure 5A) for 3 h, and then samples were irradiated with an 808 nm laser and compared with free IR-820 having the identical dye concentration. Cells without any treatment were used as a control throughout the treatment experiments (Figure 6A). The combination of IR-820 PLGA NPs and laser exposure for 30 s resulted in significant phototoxicity having 70% and 42% cell viability after 24 h post-treatment as measured by an MTT assay for 5.3 and 14.1 W/cm^2 laser power density, respectively, while 77% and 56% cell viability were observed for free IR-820 under similar conditions before and after laser illumination. We note that the laser alone or laser + PLGA NPs (without dye) has no noticeable effect on the viability of cells. These data when taken together with aqueous photothermal efficiency data from Figure 6 showed that 14.1 W/cm^2 is optimal for the IR-820-assisted photothermal therapy of cancer in vitro. Additionally, we evaluated the concentration-dependent phototoxicity at 14.1 W/cm^2 while varying the IR-820 concentration in samples, both free IR-820 and IR-820 PLGA NPs, from 1.5 to 65 μM as shown in Figure 6B. With the increase in IR-820 content, the increase in IR-820-assisted phototoxicity was observed after laser exposure as measured by MTT. At lower concentrations of dye, we do not see much difference in the phototoxicity pattern. However, the IR-820 PLGA NPs produced significant phototoxicity at the concentrations of 16−65 μM when compared with its free dye counterpart (Figure 6B).

Evaluation of the Mechanism for IR-820 PLGA NPs Induced Phototoxicity. After the successful PTT in vitro using IR-820 PLGA NPs, we next evaluated the mechanism of cell death by identifying the percentage of cells undergoing apoptosis versus necrosis using FACS study. Apoptosis is a preferred programmed cell death pathway in a normal physiologic process characterized by certain morphological features, including loss of plasma membrane asymmetry and attachment, condensation of cytoplasm and nucleus, and internucleosomal cleavage of DNA.[30] In apoptotic cells, the membrane phospholipid phosphatidylserine (PS) is translocated from the inner to the outer leaflet of the plasma membrane, thereby exposing PS to the external cellular environment, which upon treatment with Annexin V conjugated to fluorochromes including FIT-C, 35−36 kDa Ca^{2+}-dependent phospholipid-binding protein that has a high affinity for PS, binds to cells with exposed PS.[49] This format retains its high affinity for PS and thus serves as a sensitive probe for a flow cytometric analysis of cells that are undergoing apoptosis. FIT-C Annexin V staining leads to the loss of membrane integrity, which accompanies the latest stages of cell death resulting from either apoptotic or necrotic processes. Therefore, we stained with FIT-C Annexin V in conjunction with PI to identify early apoptotic cells (PI negative, FIT-C Annexin V positive). Thus, we assessed the mechanism of cell death by first treating cells with no treatment versus 20 μM of IR-820 in IR-820 PLGA NPs for 3 h and then irradiating the samples with 808 nm light for 30 s at 14.1 W/cm^2. After 24 h of incubation, cells were stained with Annexin V (FIT-C channel) and PI (PE channel) for analysis by flow cytometry. Viable cells with intact membranes exclude PI, whereas the membranes of dead and damaged cells are permeable to PI. As shown in representative scatter plots in Figure 6C, cells that stain positive for Annexin V only (bottom right quadrant Q4) are undergoing early apoptosis, while cells that stain positive for Annexin V and PI (top right quadrant Q2) are undergoing late apoptosis and cells that stain positive for PI only (top left quadrant Q1) are undergoing necrosis. The flow cytometric analysis showed that IR-820 PLGA NPs induced cell death via PTT primarily through apoptosis (52%) with no notable increase in necrotic cell percentage (0.2%) (Figure 6C). In contrast to the PTT using gold nanoparticles as seen in our previous study, the rapid and high rise in the temperature in cell suspension results in cellular necrosis where there is a reported pro-inflammatory response that can elicit a negative immune reaction that may actually promote tumor recurrence.[30,50−52] Therefore, it is essential to produce normal physiological cell death to achieve long-term survival benefits. These data when taken together with the MTT data indicate that IR-820 PLGA NPs can successfully mediate the proapoptotic PTT of breast cancer cells in vitro, warranting further investigation of its use in vivo. Furthermore, because of the limitation of the Annexin V and PI assay, which does not distinguish between cells that have undergone apoptotic death versus those that have died as a result of a necrotic pathway because, in either case, the dead cells will be stained with both Annexin V and PI, we therefore recommend that the apoptosis be measured over time so that cells can be tracked from Annexin V and PI negative (viable, or no measurable apoptosis) to Annexin V positive and PI negative (early apoptosis, membrane integrity is present) and, finally, to Annexin V and PI positive (late apoptosis and death).

CONCLUSION

In summary, we showed that IR-820 dye encapsulated into lipid polymer composite nanoparticles that are monodispersed and highly stable has optical characteristics that are maintained. The IR-820 PLGA NPs were taken up by cells and exhibited excellent biocompatibility as compared to the free IR-820 dye. However, the combination of NIR laser with IR-820 PLGA NPs has induced significant cell death when compared to its counterpart free IR-820 dye at an equivalent dye concentration. Furthermore, we confirmed the mechanism of NIR-mediated cell death is mainly via apoptosis. Considering the fact that the polymer and lipids used herein are biodegradable and Food and

https://doi.org/10.1021/acsomega.2c00306
ACS Omega 2022, 7, 12056−12065

Drug Administration (FDA)-approved biomaterials, these nanoparticles overcome the limitations of toxicity associated with metallic especially gold and iron nanoparticle-mediated thermal treatments. This study warranted further validation in in vivo PTT, and the mechanism of cell death is also essentially via apoptosis in vivo. Additionally, one could expect to compare and contrast the photothermal efficiency and mechanism of cell death of this system with gold nanoparticles for the quantitative analysis of each system. Overall, IR-820 PLGA NPs showed promise in the PTT, and these results lay the foundation for further investigation.

AUTHOR INFORMATION

Corresponding Author

Santosh Aryal − *Department of Pharmaceutical Sciences and Health Outcomes, The Ben and Maytee Fisch College of Pharmacy, The University of Texas at Tyler, Tyler, Texas 75799, United States;* orcid.org/0000-0002-7807-6342; Email: santosharyal@uttyler.edu

Author

Ramesh Marasini − *Department of Chemistry, College of Arts and Sciences, Kansas State University, Manhattan, Kansas 66506, United States; Russell H. Morgan Department of Radiology and Radiological Sciences, Division of MR Research, The Johns Hopkins University School of Medicine, Baltimore, Maryland 21205, United States; Cellular Imaging Section and Vascular Biology Program, Institute for Cell Engineering, The Johns Hopkins University School of Medicine, Baltimore, Maryland 21205, United States*

Complete contact information is available at: https://pubs.acs.org/10.1021/acsomega.2c00306

Notes

The authors declare no competing financial interest.

ACKNOWLEDGMENTS

The authors are thankful for the support from the National Institute of Biomedical Imaging and Bioengineering, National Institute of Health, under Grant No. 1R15EB030815-01. Authors thanks open access article publishing partial support from The University of Texas at Tyler. S.A. is also thankful for the support from Kansas State University (KSU) during his time at KSU.

REFERENCES

(1) Dykman, L.; Khlebtsov, N. Gold Nanoparticles in Biomedical Applications: Recent Advances and Perspectives. *Chem. Soc. Rev.* **2012**, *41* (6), 2256−2282.

(2) Sztandera, K.; Gorzkiewicz, M.; Klajnert-Maculewicz, B. Nanocarriers in Photodynamic Therapy-in Vitro and in Vivo Studies. *Wiley Interdiscip. Rev. Nanomed. Nanobiotechnol.* **2020**, *12* (3), e1509.

(3) Castano, A. P.; Mroz, P.; Hamblin, M. R. Photodynamic Therapy and Anti-Tumour Immunity. *Nat. Rev. Cancer* **2006**, *6* (7), 535−545.

(4) Zhu, H.; Cheng, P.; Chen, P.; Pu, K. Recent Progress in the Development of Near-Infrared Organic Photothermal and Photodynamic Nanotherapeutics. *Biomater. Sci.* **2018**, *6* (4), 746−765.

(5) Eustis, S.; El-Sayed, M. A. Why Gold Nanoparticles Are More Precious than Pretty Gold: Noble Metal Surface Plasmon Resonance and Its Enhancement of the Radiative and Nonradiative Properties of Nanocrystals of Different Shapes. *Chem. Soc. Rev.* **2006**, *35* (3), 209−217.

(6) Shanmugam, V.; Selvakumar, S.; Yeh, C.-S. Near-Infrared Light-Responsive Nanomaterials in Cancer Therapeutics. *Chem. Soc. Rev.* **2014**, *43* (17), 6254−6287.

(7) Zaharie-Butucel, D.; Potara, M.; Suarasan, S.; Licarete, E.; Astilean, S. Efficient Combined Near-Infrared-Triggered Therapy: Phototherapy over Chemotherapy in Chitosan-Reduced Graphene Oxide-IR820 Dye-Doxorubicin Nanoplatforms. *J. Colloid Interface Sci.* **2019**, *552*, 218−229.

(8) Huang, X.; El-Sayed, I. H.; Qian, W.; El-Sayed, M. A. Cancer Cell Imaging and Photothermal Therapy in the Near-Infrared Region by Using Gold Nanorods. *J. Am. Chem. Soc.* **2006**, *128* (6), 2115−2120.

(9) Rosensweig, R. E. Heating Magnetic Fluid with Alternating Magnetic Field. *J. Magn. Magn. Mater.* **2002**, *252*, 370−374.

(10) Thapa, P.; Li, M.; Bio, M.; Rajaputra, P.; Nkepang, G.; Sun, Y.; Woo, S.; You, Y. Far-Red Light-Activatable Prodrug of Paclitaxel for the Combined Effects of Photodynamic Therapy and Site-Specific Paclitaxel Chemotherapy. *J. Med. Chem.* **2016**, *59* (7), 3204−3214.

(11) Huang, P.; Rong, P.; Jin, A.; Yan, X.; Zhang, M. G.; Lin, J.; Hu, H.; Wang, Z.; Yue, X.; Li, W.; Niu, G.; Zeng, W.; Wang, W.; Zhou, K.; Chen, X. Dye-Loaded Ferritin Nanocages for Multimodal Imaging and Photothermal Therapy. *Adv. Mater.* **2014**, *26* (37), 6401−6408.

(12) Masotti, A.; Vicennati, P.; Boschi, F.; Calderan, L.; Sbarbati, A.; Ortaggi, G. A Novel Near-Infrared Indocyanine Dye−Polyethylenimine Conjugate Allows DNA Delivery Imaging in Vivo. *Bioconjugate Chem.* **2008**, *19* (5), 983−987.

(13) Yen, S. K.; Jańczewski, D.; Lakshmi, J. L.; Dolmanan, S. B.; Tripathy, S.; Ho, V. H. B.; Vijayaragavan, V.; Hariharan, A.; Padmanabhan, P.; Bhakoo, K. K.; Sudhaharan, T.; Ahmed, S.; Zhang, Y.; Tamil Selvan, S. Design and Synthesis of Polymer-Functionalized NIR Fluorescent Dyes−Magnetic Nanoparticles for Bioimaging. *ACS Nano* **2013**, *7* (8), 6796−6805.

(14) James, N. S.; Chen, Y.; Joshi, P.; Ohulchanskyy, T. Y.; Ethirajan, M.; Henary, M.; Strekowsk, L.; Pandey, R. K. Evaluation of Polymethine Dyes as Potential Probes for Near Infrared Fluorescence Imaging of Tumors: Part - 1. *Theranostics* **2013**, *3* (9), 692−702.

(15) Harrison, V. S. R.; Carney, C. E.; Macrenaris, K. W.; Meade, T. J. A Multimeric MR-Optical Contrast Agent for Multimodal Imaging. *Chem. Commun.* **2014**, *50* (78), 11469−11471.

(16) Harrison, V. S. R.; Carney, C. E.; MacRenaris, K. W.; Waters, E. A.; Meade, T. J. Multimeric Near IR−MR Contrast Agent for Multimodal In Vivo Imaging. *J. Am. Chem. Soc.* **2015**, *137* (28), 9108−9116.

(17) Weissleder, R.; Ntziachristos, V. Shedding Light onto Live Molecular Targets. *Nat. Med.* **2003**, *9* (1), 123−128.

(18) Berezin, M. Y.; Lee, H.; Akers, W.; Achilefu, S. Near Infrared Dyes as Lifetime Solvatochromic Probes for Micropolarity Measurements of Biological Systems. *Biophys. J.* **2007**, *93* (8), 2892−2899.

(19) Conceição, D. S.; Ferreira, D. P.; Ferreira, L. F. V. Photochemistry and Cytotoxicity Evaluation of Heptamethinecyanine Near Infrared (NIR) Dyes. *Int. J. Mol. Sci.* **2013**, *14* (9), 18557−18571.

(20) Saxena, V.; Sadoqi, M.; Shao, J. Degradation Kinetics of Indocyanine Green in Aqueous Solution. *J. Pharm. Sci.* **2003**, *92* (10), 2090−2097.

(21) Feng, Z.; Yu, X.; Jiang, M.; Zhu, L.; Zhang, Y.; Yang, W.; Xi, W.; Li, G.; Qian, J. Excretable IR-820 for *in Vivo* NIR-II Fluorescence Cerebrovascular Imaging and Photothermal Therapy of Subcutaneous Tumor. *Theranostics* **2019**, *9* (19), 5706−5719.

(22) Chen, Y.; Li, Z.; Wang, H.; Wang, Y.; Han, H.; Jin, Q.; Ji, J. IR-780 Loaded Phospholipid Mimicking Homopolymeric Micelles for Near-IR Imaging and Photothermal Therapy of Pancreatic Cancer. *ACS Appl. Mater. Interfaces* **2016**, *8* (11), 6852−6858.

(23) Kumar, P.; Srivastava, R. IR 820 Stabilized Multifunctional Polycaprolactone Glycol Chitosan Composite Nanoparticles for Cancer Therapy. *RSC Adv.* **2015**, *5* (69), 56162−56170.

(24) Srinivasan, S.; Manchanda, R.; Fernandez-Fernandez, A.; Lei, T.; McGoron, A. J. Near-Infrared Fluorescing IR820-Chitosan Conjugate for Multifunctional Cancer Theranostic Applications. *J. Photochem. Photobiol., B* **2013**, *119*, 52−59.

(25) Prajapati, S. I.; Martinez, C. O.; Bahadur, A. N.; Wu, I. Q.; Zheng, W.; Lechleiter, J. D.; McManus, L. M.; Chisholm, G. B.; Michalek, J. E.; Shireman, P. K.; Keller, C. Near-Infrared Imaging of Injured Tissue in Living Subjects Using IR-820. *Mol. Imaging* **2009**, *8* (1), 45−54.
(26) James, N. S.; Ohulchanskyy, T. Y.; Chen, Y.; Joshi, P.; Zheng, X.; Goswami, L. N.; Pandey, R. K. Comparative Tumor Imaging and PDT Efficacy of HPPH Conjugated in the Mono- and Di-Forms to Various Polymethine Cyanine Dyes: Part - 2. *Theranostics* **2013**, *3* (9), 703−718.
(27) Pandey, R. K.; James, N.; Chen, Y.; Dobhal, M. P. Cyanine Dye-Based Compounds for Tumor Imaging With and Without Photodynamic Therapy. In *Heterocyclic Polymethine Dyes: Synthesis, Properties and Applications;* Strekowski, L., Ed.; Topics in Heterocyclic Chemistry; Springer: Berlin, Germany, 2008; pp 41−74. DOI: 10.1007/7081_2008_113.
(28) Yen, S. K.; Jańczewski, D.; Lakshmi, J. L.; Dolmanan, S. B.; Tripathy, S.; Ho, V. H. B.; Vijayaragavan, V.; Hariharan, A.; Padmanabhan, P.; Bhakoo, K. K.; Sudhaharan, T.; Ahmed, S.; Zhang, Y.; Tamil Selvan, S. Design and Synthesis of Polymer-Functionalized NIR Fluorescent Dyes−Magnetic Nanoparticles for Bioimaging. *ACS Nano* **2013**, *7* (8), 6796−6805.
(29) Srinivasan, S.; Manchanda, R.; Fernandez-Fernandez, A.; Lei, T.; McGoron, A. J. Near-Infrared Fluorescing IR820-Chitosan Conjugate for Multifunctional Cancer Theranostic Applications. *J. Photochem. Photobiol., B* **2013**, *119*, 52−59.
(30) Melamed, J. R.; Edelstein, R. S.; Day, E. S. Elucidating the Fundamental Mechanisms of Cell Death Triggered by Photothermal Therapy. *ACS Nano* **2015**, *9* (1), 6−11.
(31) Pitchaimani, A.; Nguyen, T. D. T.; Aryal, S. Natural Killer Cell Membrane Infused Biomimetic Liposomes for Targeted Tumor Therapy. *Biomaterials* **2018**, *160*, 124−137.
(32) Abello, J.; Nguyen, T. D. T.; Marasini, R.; Aryal, S.; Weiss, M. L. Biodistribution of Gadolinium- and near Infrared-Labeled Human Umbilical Cord Mesenchymal Stromal Cell-Derived Exosomes in Tumor Bearing Mice. *Theranostics* **2019**, *9* (8), 2325−2345.
(33) Nguyen, T. D. T.; Aryal, S.; Pitchaimani, A.; Park, S.; Key, J.; Aryal, S. Biomimetic Surface Modification of Discoidal Polymeric Particles. *Nanomedicine Nanotechnol. Biol. Med.* **2019**, *16*, 79−87.
(34) Hu, C.-M. J.; Kaushal, S.; Cao, H. S. T.; Aryal, S.; Sartor, M.; Esener, S.; Bouvet, M.; Zhang, L. Half-Antibody Functionalized Lipid−Polymer Hybrid Nanoparticles for Targeted Drug Delivery to Carcinoembryonic Antigen Presenting Pancreatic Cancer Cells. *Mol. Pharmaceutics* **2010**, *7* (3), 914−920.
(35) Marasini, R.; Thanh Nguyen, T. D.; Aryal, S. Integration of Gadolinium in Nanostructure for Contrast Enhanced-Magnetic Resonance Imaging. *WIREs Nanomedicine Nanobiotechnology* **2020**, *12* (1), No. e1580.
(36) Marasini, R.; Rayamajhi, S.; Moreno-Sanchez, A.; Aryal, S. Iron(Iii) Chelated Paramagnetic Polymeric Nanoparticle Formulation as a next-Generation T 1 -Weighted MRI Contrast Agent. *RSC Adv.* **2021**, *11* (51), 32216−32226.
(37) Nguyen, T. D. T.; Marasini, R.; Aryal, S. Re-Engineered Imaging Agent Using Biomimetic Approaches. *WIREs Nanomedicine Nanobiotechnology* **2022**, *14* (1), No. e1762.
(38) Ferrel, C.; Rayamajhi, S.; Nguyen, T.; Marasini, R.; Saravanan, T.; Deba, F.; Aryal, S. Re-Engineering a Liposome with Membranes of Red Blood Cells for Drug Delivery and Diagnostic Applications. *ACS Appl. Bio Mater.* **2021**, *4* (9), 6974−6981.
(39) Marasini, R.; Nguyen, T. D. T.; Rayamajhi, S.; Aryal, S. Synthesis and Characterization of a Tumor-Seeking LyP-1 Peptide Integrated Lipid−Polymer Composite Nanoparticle. *Mater. Adv.* **2020**, *1* (3), 469−480.
(40) Pitchaimani, A.; Nguyen, T. D. T.; Marasini, R.; Eliyapura, A.; Azizi, T.; Jaberi-Douraki, M.; Aryal, S. Biomimetic Natural Killer Membrane Camouflaged Polymeric Nanoparticle for Targeted Bioimaging. *Adv. Funct. Mater.* **2019**, *29* (4), 1806817.
(41) Marasini, R.; Nguyen, T.; Rayamajhi, S.; Aryal, S. Interaction of Tumor Homing LyP-1 Peptide Designed as Lipid-Polymer Hybrid Nanoparticle with Overexpressed Cell Surface Protein P32 Using Osteosarcoma Tumor Model. In *Chemical Biology and Interfaces;* American Chemical Society: Washington, DC, 2019; Vol. *257*.
(42) Aryal, S.; Nguyen, T.; Pithchaimani, A.; Marasni, R. Biologically Inspired Design Consideration for Polymeric Anticancer Nanomedicine. In *Colloids and Interfaces;* American Chemical Society: Washington, DC, 2018; Vol. *256*.
(43) Pitchaimani, A.; Nguyen, T. D. T.; Koirala, M.; Zhang, Y.; Aryal, S. Impact of Cell Adhesion and Migration on Nanoparticle Uptake and Cellular Toxicity. *Toxicol. In Vitro* **2017**, *43*, 29−39.
(44) Nguyen, T. D. T.; Pitchaimani, A.; Aryal, S. Engineered Nanomedicine with Alendronic Acid Corona Improves Targeting to Osteosarcoma. *Sci. Rep.* **2016**, *6* (1), 36707.
(45) Pridgen, E. M.; Langer, R.; Farokhzad, O. C. Biodegradable, Polymeric Nanoparticle Delivery Systems for Cancer Therapy. *Nanomed* **2007**, *2* (5), 669−680.
(46) Rayamajhi, S.; Marchitto, J.; Nguyen, T. D. T.; Marasini, R.; Celia, C.; Aryal, S. PH-Responsive Cationic Liposome for Endosomal Escape Mediated Drug Delivery. *Colloids Surf. B Biointerfaces* **2020**, *188*, 110804.
(47) Nguyen, T. D. T.; Marasini, R.; Rayamajhi, S.; Aparicio, C.; Biller, D.; Aryal, S. Erythrocyte Membrane Concealed Paramagnetic Polymeric Nanoparticle for Contrast-Enhanced Magnetic Resonance Imaging. *Nanoscale* **2020**, *12* (6), 4137−4149.
(48) Aryal, S.; Rayamajhi, S.; Nguyen, T.; Marasini, R. Re-Engineering Immuno-Exosome as Theranostics. In *Abstracts of Papers of the American Chemical Society;* American Chemical Society: Washington, DC, 2019; Vol. *258*.
(49) Shi, C.; Wu, J. B.; Pan, D. Review on Near-Infrared Heptamethine Cyanine Dyes as Theranostic Agents for Tumor Imaging, Targeting, and Photodynamic Therapy. *J. Biomed. Opt.* **2016**, *21* (5), 050901.
(50) Marasini, R.; Pitchaimani, A.; Nguyen, T. D. T.; Comer, J.; Aryal, S. The Influence of Polyethylene Glycol Passivation on the Surface Plasmon Resonance Induced Photothermal Properties of Gold Nanorods. *Nanoscale* **2018**, *10* (28), 13684−13693.
(51) Pérez-Hernández, M.; del Pino, P.; Mitchell, S. G.; Moros, M.; Stepien, G.; Pelaz, B.; Parak, W. J.; Gálvez, E. M.; Pardo, J.; de la Fuente, J. M. Dissecting the Molecular Mechanism of Apoptosis during Photothermal Therapy Using Gold Nanoprisms. *ACS Nano* **2015**, *9* (1), 52−61.
(52) Bear, A. S.; Kennedy, L. C.; Young, J. K.; Perna, S. K.; Mattos Almeida, J. P.; Lin, A. Y.; Eckels, P. C.; Drezek, R. A.; Foster, A. E. Elimination of Metastatic Melanoma Using Gold Nanoshell-Enabled Photothermal Therapy and Adoptive T Cell Transfer. *PLoS One* **2013**, *8* (7), No. e69073.

https://doi.org/10.1021/acsomega.2c00306
ACS Omega 2022, 7, 12056−12065